

Full-Depth Global Estimates of Ocean Mesoscale Eddy Mixing from Observations and Theory

Sjoerd Groeskamp¹, Joseph H. LaCasce², Trevor J. McDougall³, Marine Rogé⁴

¹NIOZ Royal Netherlands Institute for Sea Research, P.O. Box 59, 1790 AB, Den Burg, Texel, The Netherlands

²Department of Geosciences, University of Oslo, Oslo, Norway.

³School of Mathematics and Statistics, University of New South Wales, Sydney, Australia.

⁴Climate Change Research Centre, University of New South Wales, Sydney, Australia.

Key Points:

- A new parameterisation for mesoscale eddy mixing that combines mixing-length and flow-suppression theory with vertical modes.
- Global, full-depth mesoscale eddy mixing estimates are obtained from observations of temperature, salinity, pressure and eddy kinetic energy.
- Mesoscale eddy mixing is surface intensified and strongly influenced by the vertical stratification of ocean density.

Corresponding author: Sjoerd Groeskamp, sjoerdgroeskamp@gmail.com

Abstract

Mixing by mesoscale eddies profoundly impacts climate and ecosystems by redistributing and storing dissolved tracers such as heat and carbon. Eddy mixing is parameterized in most numerical models of the ocean and climate. To reduce known sensitivity to such parameterizations, observational estimates of mixing are needed. However, logistical and technological limitations obstruct our ability to measure global time-varying mixing rates. Here, we extend mixing length theory with mean-flow suppression theory, and first surface modes, to estimate mixing from readily-available observational-based climatological data, of salinity, temperature, pressure and eddy kinetic energy at the sea surface. The resulting full-depth global maps of eddy mixing can reproduce the few available direct estimates and confirm the importance of mean-flow suppression of mixing. The results also emphasize the significant effect of eddy surface intensification and its relation to the vertical density stratification. These new insights in mixing dynamics will improve future mesoscale eddy mixing parameterizations.

Plain Language Summary

Large whirls of hundreds of kilometers can mix water with different temperatures, salinity and other properties. These whirls are called “mesoscale eddies” and are very difficult to include in numerical simulation of ocean and climate. Therefore, we include them using a simplified representation: a parameterization. These parameterizations need as input, the strength with which these eddies mix. Ideally, we would thus measure these mixing strengths globally and over the full depth of the ocean. However, this is impossible due to technological, logistical and financial limitations. To avoid these limitations, we instead indirectly estimate mixing from variables that we can measure globally over the full depth of the ocean. We here present a new way to indirectly estimate mixing from widely available observations of temperature, salinity, pressure and surface eddy kinetic energy. This results in 3-dimensional maps of eddy mixing strengths. We find that eddies mix much stronger near the surface than in the deep ocean, and that this is partly caused by the vertical stratification of ocean density. These new insights and maps can be used to improve mixing parameterizations and thus significantly improve all kinds of calculations that are important for the Earth’s climate and ecosystems.

1 Introduction

Instability of the large-scale density field produces geostrophically-balanced, mesoscale ocean eddies (Gill et al., 1974; Wunsch & Ferrari, 2004), which are central for ocean mass and tracer transport (Gnanadesikan et al., 2015; Busecke & Abernathey, 2019; Jones & Abernathey, 2019; Busecke et al., 2014). The eddies vary in size from kilometers to hundreds of kilometers and as such are unresolved in many global ocean and climate models (Chelton et al., 1998). The eddies are accordingly parameterized in the models (Meijers, 2014; Fox-Kemper et al., 2019; Jansen et al., 2019; Hallberg, 2013). But the simulations are often sensitive to the choice of parameterizations (Jones & Abernathey, 2019; Ferreira et al., 2005; Sijp et al., 2006; Pradal & Gnanadesikan, 2014).

Having proper three dimensional observations of eddy mixing would greatly aid in the choice of parameterizations, reducing model uncertainty. Direct observations have been made in tracer release experiments (Ledwell et al., 1993, 1998), and also estimated using Lagrangian drifters and subsurface floats (Zhurbas & Oh, 2004; LaCasce et al., 2014; Roach et al., 2018), satellite data (Holloway, 1986; R. P. Abernathey & Marshall, 2013; Klocker & Abernathey, 2013; Busecke & Abernathey, 2019), hydrographic data (Chapman & Sallée, 2017), inverse methods (Zika et al., 2010; Groeskamp et al., 2017; Hautala, 2018) and salinity anomalies (Cole et al., 2015). These studies have significantly increased our understanding of eddy size, eddy kinetic energy (EKE) and mixing suppression by mean flows. Broadly speaking, the studies indicate enhanced mixing near western boundary currents and the

67 Antarctic Circumpolar Current, and reduced mixing in the eastern subtropical-gyres and
 68 at high latitudes. However, almost none of these observational-based studies offer global
 69 and/or full-depth coverage; rather they are local, confined to the surface, or limited to the
 70 area significantly sampled by Argo floats. The one global study that we know of provides
 71 only estimates integrated over the mixed layer and the abyss (Groeskamp et al., 2017).

72 Here we propose a method to estimate eddy mixing using satellite observations and
 73 readily available observations of Absolute Salinity S_A , Conservative Temperature Θ , pres-
 74 sure p and the surface EKE. This involves projecting the surface velocities to depth using
 75 recently-derived vertical structure functions. The resulting global, full-depth diffusivity
 76 maps agree well with previous observations and indirect estimates. The vertical density
 77 stratification (N^2) dictates the extent of surface intensification of eddy mixing and, in turn,
 78 of mixing at depth. These new insights will aid the next steps in understanding, constructing
 79 and constraining eddy mixing parameterizations.

80 2 The eddy diffusivity parameterizations

81 We here study the mixing by along-isopycnal diffusion of passive tracers by mesoscale
 82 eddies, which we represent with a turbulent isopycnal mesoscale eddy diffusivity K . The
 83 foundation is an estimate based on mixing length theory (Prandtl, 1925):

$$84 \quad K_{\text{MLT}} = \Gamma u_{\text{rms}} L_{\text{mix}} \quad (1)$$

85 Here Γ is the mixing efficiency, u_{rms} the rms geostrophic velocity and L_{mix} the mixing length
 86 scale. Such a relation has been used for both atmospheric (Bretherton, 1966) and oceanic
 87 modelling (Holloway, 1986; Marshall & Adcroft, 2010; R. P. Abernathy & Marshall, 2013;
 88 Klocker & Abernathy, 2013; Naveira Garabato et al., 2015). Following the realization that
 89 mixing is suppressed in the presence of a mean flow, the above estimate was modified. For
 90 the case of a zonal mean flow, this is (Ferrari & Nikurashin, 2010; Klocker et al., 2012):

$$91 \quad K = \frac{K_{\text{MLT}}}{1 + k^2 \gamma^{-2} (c_w - U)^2} \quad (2)$$

92 Here γ is the reciprocal of an eddy decorrelation time (s^{-1}), k the zonal (eddy) wavenumber,
 93 c_w an eddy drift speed and U the mean velocity.

94 2.1 Depth Dependent K_{MLT}

95 Eq. (2) has been applied previously at the sea surface (Klocker & Abernathy, 2013),
 96 but here we extend it to depth by using the depth-dependent velocity $U = U(z)$ in the
 97 denominator (Ferrari & Nikurashin, 2010; Klocker et al., 2012). The velocity can be obtained
 98 from integrating the thermal wind relation downward from the sea surface. K_{MLT} also
 99 depends on depth, through its dependence on u_{rms} . Assuming the vertical structure is
 100 separable, the components of the eddy velocity can be expressed as $(u', v') = \phi(z) (u'_0, v'_0)$,
 101 where $\phi(z)$ is a vertical structure function and the zero subscript velocities are the surface
 102 values. The $u_{\text{rms}}(z)$ is then given by:

$$103 \quad u_{\text{rms}} = \sqrt{(u'^2 + v'^2)} = \phi(z) \sqrt{2\text{EKE}_0}, \quad (3)$$

104 which can be obtained from the surface EKE_0 .

105 The function $\phi(z)$ in turn can be found by solving a vertical structure equation which
 106 has the vertical stratification N^2 as the only input (Charney, 1971; Gill, 1982; Wunsch,
 107 2015). The resulting eigenmodes (the "baroclinic modes") were traditionally found assum-
 108 ing a flat bottom boundary. The first baroclinic mode is familiar in oceanography, having
 109 opposed flow at the surface and bottom. However, observations from current meters sug-
 110 gest that bathymetry affects time-dependent motion throughout the water column, in most

111 regions of the ocean (de La Lama et al., 2016). This can be taken into account by impos-
 112 ing a no horizontal flow condition at the bottom, i.e. $\phi(z = -H) = 0$ (LaCasce, 2017).
 113 The gravest resulting ϕ (the "first surface mode") closely resembles the gravest empirical
 114 orthogonal function from the current meter observations (de La Lama et al., 2016; LaCasce
 115 & Groeskamp, 2020). The latter accounts for more than 50% of the variance in many lo-
 116 cations. Thus we use the first surface mode to represent the dominant vertical structure of
 117 the horizontal geostrophic eddies (Appendix B).

118 Bottom-trapped (topographic wave) modes (Rhines, 1970; Thompson & Luyten, 1976)
 119 may also contribute significantly to subsurface mixing. Such modes have a maximum near
 120 the bottom that decays with height, and the associated mixing would be similarly bottom-
 121 intensified. However, it is presently unknown how to estimate the topographic wave field
 122 from surface data (or if that is even possible). This is should be the subject of future work.

123 We must also specify the mixing length, L_{mix} (Eq. 1). A consistent choice is the
 124 first Rossby radius of deformation, L_d , the eigenvalue associated with the first baroclinic
 125 mode. Ocean eddies propagate westward, in most regions outside of the Southern Ocean
 126 (where, due to advection by the Antarctic Circumpolar Current, they drift eastward instead)
 127 (Chelton & Schlax, 1996; Chelton et al., 1998). The propagation speed is consistent with
 128 that of long Rossby waves, if one uses the deformation radius associated with the first surface
 129 mode (LaCasce & Groeskamp, 2020). As such, the surface mode radius is a reasonable choice
 130 for eddy scale.

131 The radius, which is inversely proportional to the Coriolis parameter, becomes infinite
 132 at the equator. Thus one uses an alternate estimate, based on the "equatorial beta plane",
 133 at low latitudes (Chelton et al., 1998). Specifically, we use the expression of Hallberg (2013):

$$134 \quad L_d = \frac{c_1}{\sqrt{f^2 + 2c_1\beta}}. \quad (4)$$

135 where c_1 is the first surface mode gravity wave phase speed, f is the Coriolis parameter and
 136 $\beta = df/dy$ is its latitudinal gradient.

137 2.2 The Suppression Factor

138 Estimates of c_w (Eq. 2) are often made using Hovmöller diagrams of the sea surface
 139 height. Instead, we exploit the fact that over most of the ocean eddy drift speeds are
 140 well-approximated by the surface mode phase speed, Doppler shifted by the time- and
 141 depth-averaged velocity (Klocker & Abernathy, 2013; Klocker & Marshall, 2014; Chapman
 142 & Sallée, 2017). This yields $\mathbf{c}_w(x, y) = (\bar{U}^{z,t} - \beta L_d^2, \bar{V}^{z,t})$. Again, the velocities U and V
 143 are obtained from thermal wind, and L_d is the first surface radius. An alternate expression
 144 can be obtained assuming a two layer ocean (Wang et al., 2016), but the present version
 145 is more appropriate with continuous stratification. Finally, we write the wavenumber as
 146 $k = 2\pi/L_d$. Taken together, this yields:

$$147 \quad K = \underbrace{\Gamma \phi(z) \sqrt{2\text{EKE}_0}}_{K_{\text{MLT}}} L_d \times \min(S^x, S^y), \quad (5)$$

148 with

$$149 \quad S_x = \frac{1}{1 + \frac{4\pi^2}{\gamma^2 L_d^2} (\delta v)^2}, \quad S_y = \frac{1}{1 + \frac{4\pi^2}{\gamma^2 L_d^2} (\delta u - \beta L_d^2)^2}, \quad (6)$$

150 where $\delta v = \bar{v}^{z,t} - v(z)$ and $\delta u = \bar{u}^{z,t} - u(z)$. Note that U_0 and V_0 have cancelled out,
 151 avoiding the introduction of errors through an estimate of the surface velocity. As such, δu
 152 and δv are entirely determined from hydrography, (S_A, Θ, p) .

153 Suppression theory provides a means for estimating cross-stream diffusivities, as along-
 154 stream transport is dominated by advection (Ferrari & Nikurashin, 2010). Following Klocker

155 and Abernathey (2013); Chapman and Sallée (2017), we use the minimum suppression factor,
 156 i.e. $\min(S^x, S^y)$, rather than the value perpendicular to the large-scale mean flow
 157 (Zhurbas & Oh, 2004). The latter was attempted, but yielded noisier results due to un-
 158 certainties in the rotation angle. Finally, we note that γ is used as a fitting parameter, as
 159 discussed later.

160 3 Collecting the ingredients

161 Thus we require only observations of S_A , Θ , p and EKE_0 to calculate K . The former
 162 were obtained from annual mean fields from the World Ocean Atlas 2018 (Garcia et
 163 al., 2019), gridded climatology, while the EKE_0 comes from CMEMS (Copernicus Marine
 164 Environment Monitoring Service) operational delayed-time sea surface geostrophic velocity
 165 anomalies derived from satellite altimetry (Pujol et al., 2016; Taburet et al., 2019) (Ap-
 166 pendix A). The mixing parameter was set to be $\Gamma = 0.35$ (Klocker & Abernathey, 2013).

167 The decay rate, γ , was obtained by fitting K to the diffusivity estimates obtained
 168 from the North Atlantic Tracer Release Experiment (NATRE) and Diapycnal and Isopycnal
 169 Mixing Experiment in the Southern Ocean (DIMES). The parameter was found via a least
 170 squares fit using both sets of data (using only estimates indicated with black colors in Fig.
 171 1). We find $\gamma^{-1} = 1.68$ days, which is comparable to, but also somewhat smaller than the
 172 4 days found previously for the surface (Klocker & Abernathey, 2013).

173 4 Comparing to observations

174 The resulting diffusivity profiles compare well to those obtained in NATRE and DIMES
 175 (Fig. 1). The present estimate captures the vertical decay in the NATRE profile, and also the
 176 subsurface maximum observed in the DIMES experiment. Notably, in both cases including
 177 the mean flow suppression factor significantly improves the results.

178 Other estimates are also shown for comparison. The semi-global estimates of Cole
 179 et al. (2015) somewhat overestimate the diffusivities, while the global inverse estimates
 180 of Groeskamp et al. (2017) underestimate them. An additional curve is included in each
 181 case showing the vertical structure if the traditional (flat-bottom) baroclinic mode is used
 182 instead of the surface mode (Appendix B). This yields a mid-depth minimum and thus a
 183 very different vertical structure than observed.

184 4.1 Global maps

185 The factor indicating mean flow suppression of the mixing, given in (6), is mapped in
 186 Fig. (2). Suppression is enhanced in the cores of the western boundary currents and reduced
 187 on their flanks. It is pronounced in the Antarctic Circumpolar Current, over large swaths
 188 of the Southern Ocean. Suppression is also strongly evident at low latitudes, reflecting the
 189 large deformation radius there. Suppression is correspondingly weaker in the high latitudes,
 190 where L_d is small.

191 The suppression factor helps understand the spatial variability exhibited by the diffusiv-
 192 ity, shown in Fig. 3. For example, K is weaker in the core of the Gulf Stream but enhanced
 193 to its south, while diffusivities in the equatorial region are smaller than in the subtropical
 194 gyres. Diffusivities are large in the Agulhas system, in the South Equatorial Current in the
 195 Indian Ocean and in the western Pacific. Yet, diffusivities are smaller at high latitudes as
 196 the smaller L_d yields a shorter mixing length. Previously-noted features such as the mix-
 197 ing desert in the North Pacific and Subtropical Southern Atlantic (Klocker & Abernathey,
 198 2013; R. P. Abernathey & Marshall, 2013), are also clearly seen. Meanwhile the estimates
 199 in the NATRE and DIMES regions, indicated by the squares in the eastern North Atlantic
 200 and the South Pacific, respectively, compare well to those described previously (Klocker &
 201 Abernathey, 2013; R. P. Abernathey & Marshall, 2013; Chapman & Sallée, 2017) (Fig. 1).

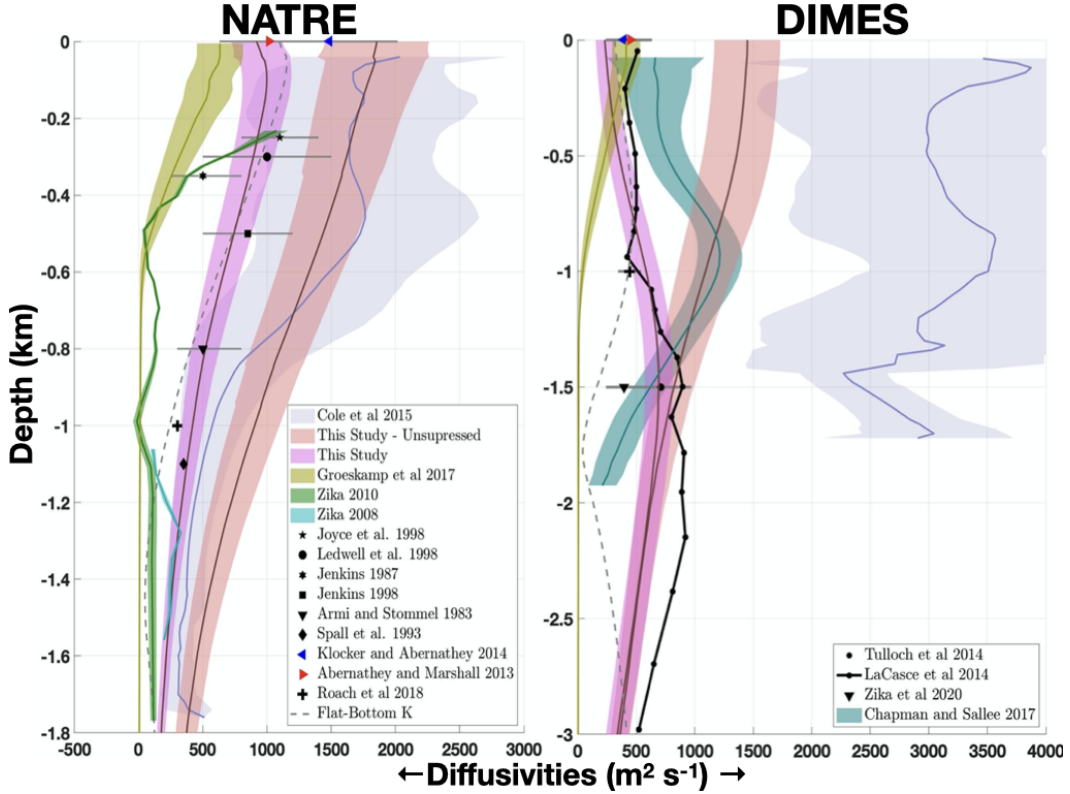


Figure 1. Comparing the present results against direct observations (black points) (Joyce et al., 1998; Ledwell et al., 1998; Jenkins, 1987, 1998; Armi & Stommel, 1983; Spall et al., 1993; Tulloch et al., 2014; Zika et al., 2020) and indirect estimates (Cole et al., 2015; Zika et al., 2010; Zika & McDougall, 2008; Klocker & Abernathy, 2013; R. P. Abernathy & Marshall, 2013; LaCasce et al., 2014; Groeskamp et al., 2017; Roach et al., 2018; Chapman & Sallée, 2017) in the NATRE (left) and DIMES (right) region.

202 Mean flow suppression also varies with depth (Fig. 2b), affecting the vertical structure
 203 of the diffusivities (Fig. 3b). Strong suppression is observed at all depths in the tropics,
 204 but suppression is intensified near the surface and weaker at depth at mid-latitudes. It is
 205 for this reason the diffusivity exhibits a subsurface maximum in for example the Southern
 206 Ocean (Fig. 3b), including the DIMES region (Fig. 1) (R. Abernathy et al., 2010; Klocker
 207 et al., 2012; LaCasce et al., 2014; Tulloch et al., 2014).

208 The vertical variation of the diffusivity also depends on the vertical structure of the
 209 eddy kinetic energy, represented by the function $\phi(z)$. As noted, this is obtained by ap-
 210 plying theoretical arguments to an observationally based gridded hydrographic climatology
 211 (LaCasce & Groeskamp, 2020). We illustrate this by mapping the depth at which ϕ has
 212 decreased by an e-folding scale from its surface value ($\phi(z) = 1/e = 0.37$, Fig. 4a), and show
 213 representative vertical profiles of $\phi(z)$ (Fig. 4b). The e-folding depth is small in shallow
 214 regions, for instance along the continental slopes. It is large where the stratification is weak,
 215 notably near Antarctica and in the Labrador Sea, and smaller where the stratification is
 216 strong, as in the subtropical gyres (10-30°N and 10-30°S). That the diffusivity is strongly
 217 surface intensified is also clear in the NATRE region (Fig. 1).

218 There is significant longitudinal variation however, for example in the South Atlantic.
 219 The larger e-folding depth in the west stems from the intrusion of Antarctic Bottom Water.

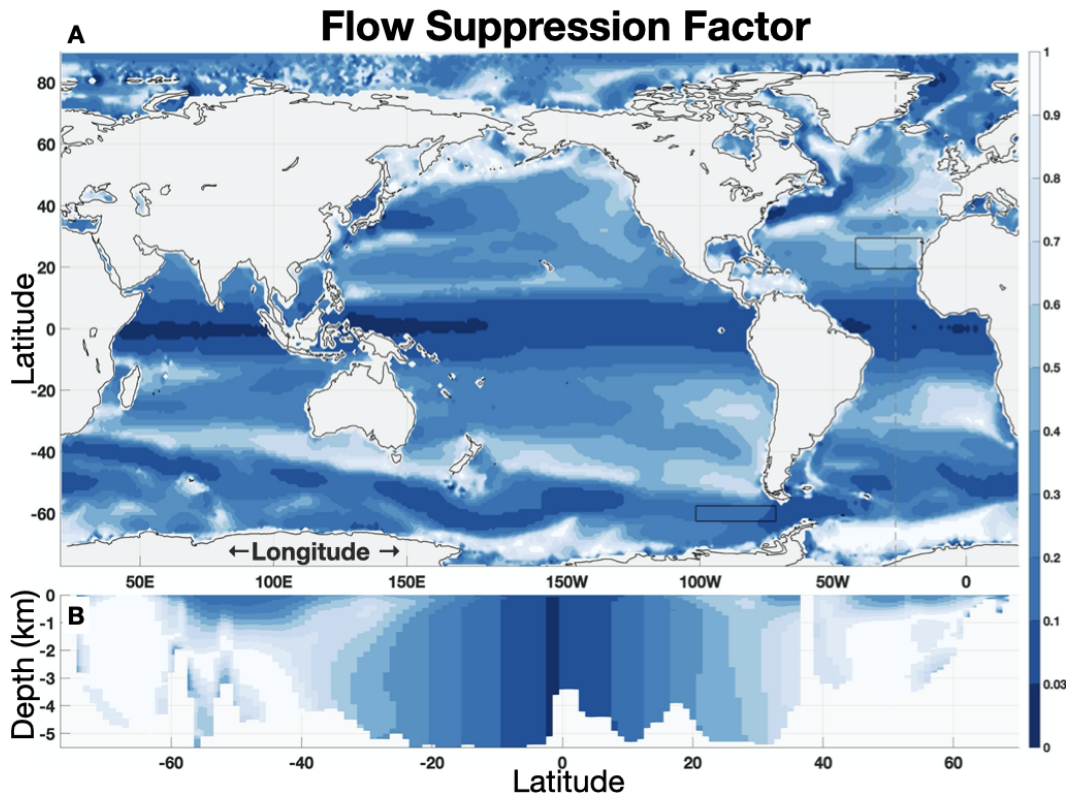


Figure 2. The suppression factor at the surface (Eq. 6) (A) and for a north-south transect in the Atlantic ocean (B), as indicated by the meridional grey dashed line in (A). NATRE and DIMES are indicated by squares.

220 This increases the deep ocean stratification, causing a more gradual vertical decay of ϕ (to
 221 satisfy the bottom boundary condition) than in the east side of the basin. This contrast
 222 is consistent with data from two WOCE current meters, at the locations indicated by the
 223 star and diamond in the map. The first Empirical Orthogonal Functions (EOF), derived
 224 from the horizontal velocities (Fig. 4b), are plotted in the insert. The eastern current
 225 meter (though just to the east of the shallow portion of the map) has an EOF which decays
 226 more rapidly with depth than the western current meter (the starred profile). This leads
 227 to stronger surface intensification in the east and thus larger mixing rates at depth in the
 228 western South Atlantic than in the east.

229 5 Summary

230 A new parametrization for the along-isopycnal mesoscale eddy diffusivity is presented.
 231 This novelty extends the Prandtl (1925) mixing length theory employing mean-flow suppres-
 232 sion theory (Ferrari & Nikurashin, 2010) and the theory of vertical modes over bathymetry
 233 (LaCasce & Groeskamp, 2020). The parameterisation is applied to widely- and readily-
 234 available observations of S_A , Θ , p and surface EKE to produce a global, full-depth map of
 235 along-isopycnal mesoscale eddy diffusivity. The estimated diffusivities exhibit strong spatial
 236 variations and are in line with previous surface estimates, and also agree well with subsurface
 237 profiles obtained from experiments in the eastern North Atlantic and the Southern Ocean.

238 The adopted surface mode vertical structure, while supported by observations, has not
 239 yet been widely adopted. An exception is the Geophysical Fluid Dynamics Laboratory

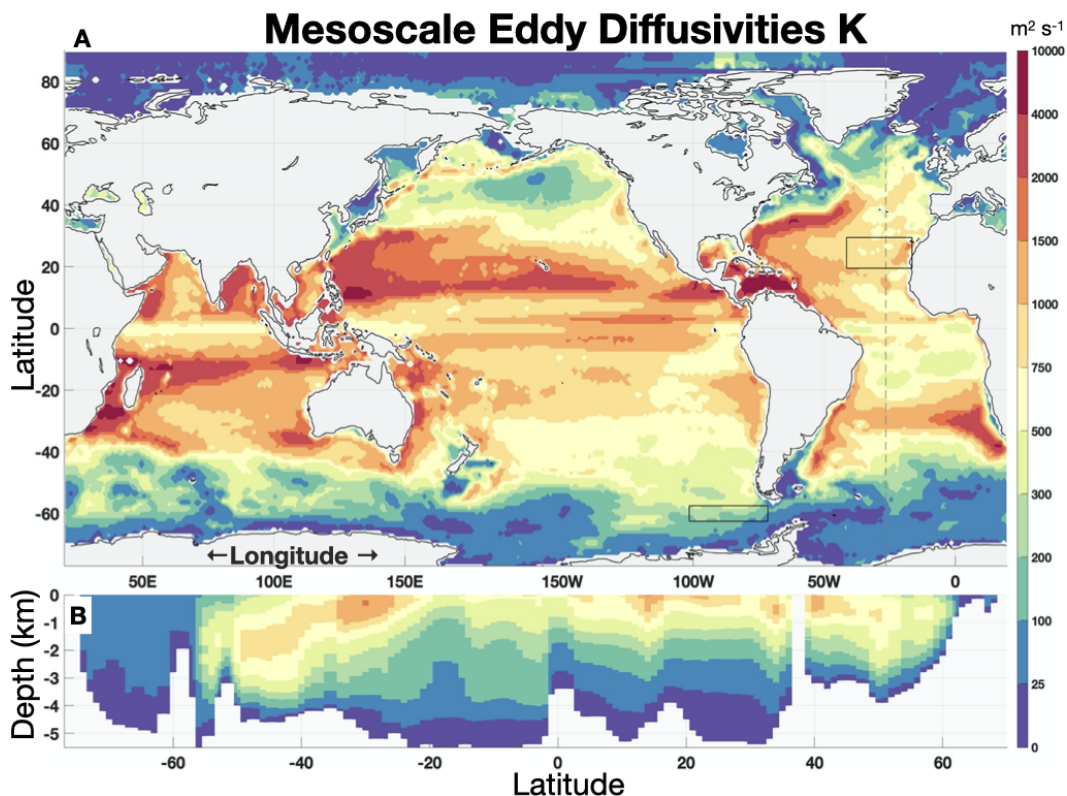


Figure 3. The diffusivity K at the ocean surface (A) and for a north-south transect in the Atlantic ocean (B) along the grey dashed line in (A). The NATRE and DIMES regions are indicated by rectangles.

240 (GFDL) OM4.0 numerical model, which employs a first baroclinic mode with no slip imposed
 241 imposed at the bottom when representing the vertical structure of the diffusivity (Adcroft
 242 et al., 2019). With strong surface stratification, relative to the abyssal stratification, the
 243 surface mode is strongly surface-intensified. This is in line with previous studies which also
 244 found indications of surface intensification (Groeskamp et al., 2017; Canuto et al., 2019).
 245 Consequently, large scale thermohaline and wind forcing that alters surface stratification
 246 determines how mixing varies with depth. Thus while eddies may alter the stratification
 247 (Dewar, 1986), stratification also impacts eddy mixing.

248 The diffusivities derived here represent mesoscale mixing of tracer (Redi, 1982), yet the
 249 same eddies also mix mass between pairs of density surfaces. This is called the temporal
 250 residual-mean velocity in height-coordinate models and bolus-velocity in density coordinate
 251 models (T. J. McDougall & McIntosh, 2001). The tracer and "mass" diffusivities are known
 252 to differ, but are related through theoretical considerations as described by Smith and
 253 Marshall (2009). Applying their theory to the presented diffusivities may provide a way
 254 forward to use the results of this study for both temporal residual-mean and bolus-velocity
 255 transports.

256 The development of mixing parameterizations that are able to respond to changing
 257 state of the ocean remains a challenge for numerical modeling (Fox-Kemper et al., 2019).
 258 The present parameterisation, based on the ocean state, provides a way forward to over-
 259 come this challenge. This will in turn much improve numerical modeling of ocean physics,
 260 biogeochemistry and future climate.

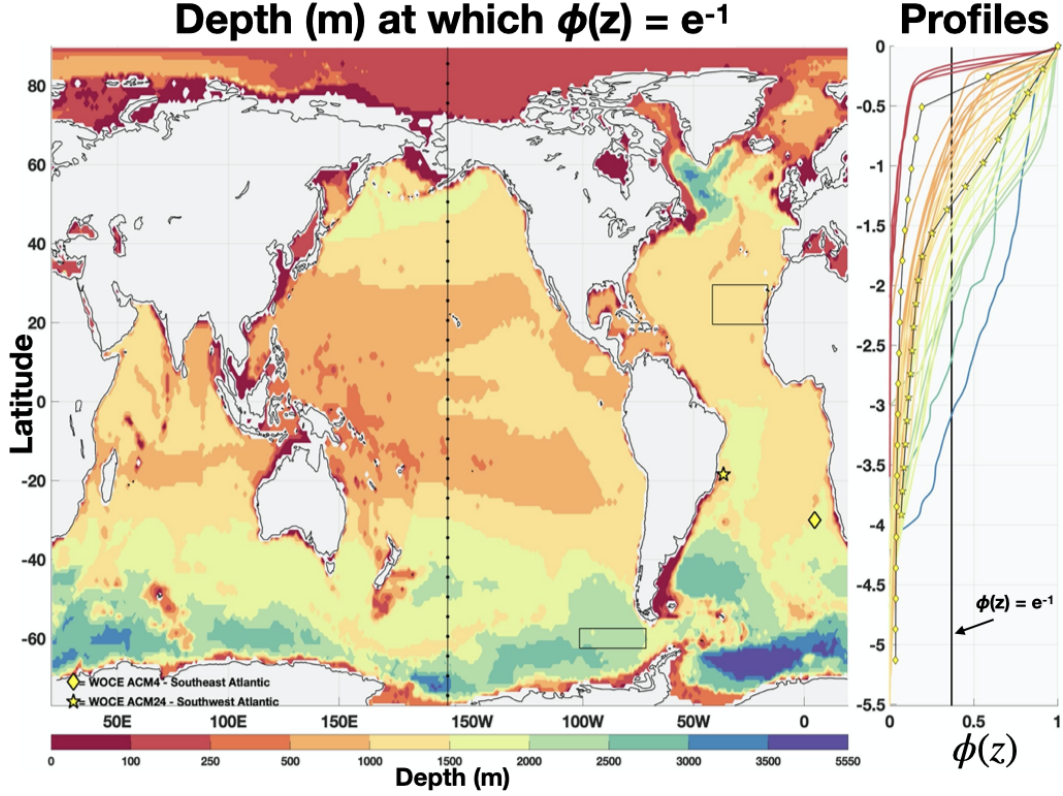


Figure 4. The e-folding depth for the geostrophic eddy velocity, i.e the depth at which $\phi(z) = 0.37$ (left). The star and diamond indicate the locations of the ACM24 (Durrieu De Madron & Weatherly, 1994) and ACM04 (Garzoli et al., 1996) current meter moorings, respectively. Examples of individual profiles of $\phi(z)$ (right). The profiles are from 160W, indicated by the black dotted line in the left panel, and the two current meters. The colors are the same as for the left panel.

261 6 Appendix A - the data

262 World Ocean Atlas *in situ* temperature and practical salinity are used to calculate
 263 Conservative Temperature Θ and Absolute Salinity S_A (T. J. McDougall, 2003; Graham &
 264 McDougall, 2013; T. J. McDougall et al., 2012; IOC et al., 2010) using the GSW software
 265 toolbox (T. McDougall & Barker, 2011), and are then interpolated to a 10 m vertical grid
 266 resolution using interpolation software of Barker and McDougall (2020). The resulting data
 267 is made statically stable using Barker and McDougall (2017), with a minimum stability
 268 given by Jackett and McDougall (1997). The resulting buoyancy frequency N^2 is smoothed
 269 with a 5-point running mean to filter out small scale oscillations.

270 The CMEMS multiple-satellite-merged data are daily, spanning from 1993 to present,
 271 and gridded at a spatial resolution of 0.25° in both zonal and meridional directions. The
 272 geostrophic currents are calculated using the geostrophic relations for latitudes outside the
 273 $\pm 5^\circ$ N band, and using a β -plane approximation of the geostrophic equations in the equatorial
 274 band (Lagerloef et al., 1999). The u_{rms} is defined here as the root mean square of the mean
 275 EKE, computed from the altimetric geostrophic velocity anomalies over the period 1993-01-
 276 01 – 2017-05-15, and is re-gridded onto the WOA grid before computing u_{rms} (Fig. 5b).

277 Current meter data is used in the East (mooring 4 of ACM04 (Garzoli et al., 1996)
 278 and West (mooring 4 of ACM24 (Durrieu De Madron & Weatherly, 1994)) Atlantic. Both
 279 moorings measure velocity at 4 depths ranging 900m to 3915m for ACM24, and from 210m

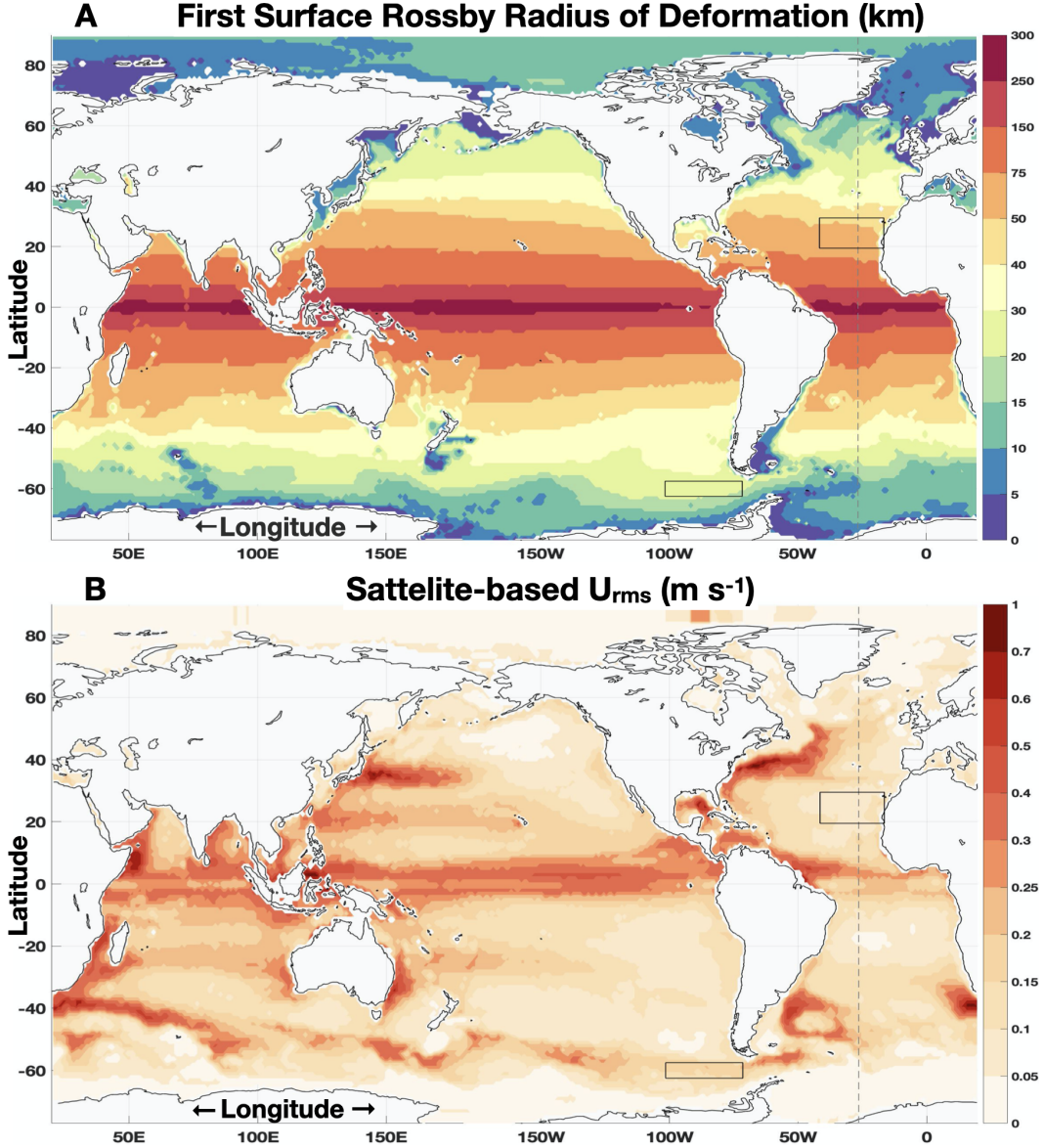


Figure 5. The first surface mode deformation radius L_d (A), and the annual mean root mean square (rms) geostrophic eddy velocity u_{rms} derived from sea surface height satellite data (B)

280 to 4092m for ACM04. The first EOF of the measured EKE explains 84% and 90% of the
 281 variance for AMC24 and AMC04, respectively. The modes are linearly interpolated to the
 282 surface, and normalised with the surface value. The results are interpreted as an indication
 283 that we find similar behaviour from observations of ocean currents as from rough-bottom
 284 modes derived using Surface Modes.

285 **7 Appendix B - Solving for Φ and L_d .**

286 The linear Quasi Geostrophic Potential Vorticity equation governs flows with small
 287 Rossby numbers. Assuming a plane wave solutions of the form $\sim \phi(z) \tilde{\Psi} e^{(ikx + iyl - i\omega t)}$
 288 yields a differential equation for the vertical structure the horizontal flow $\phi(z)$ (Gill, 1982;

289 Pedlosky, 1987; Wunsch, 2015):

$$\frac{d}{dz} \left(\frac{f_0^2}{N^2} \frac{d\phi}{dz} \right) + \frac{1}{c^2} \phi = 0, \quad \text{with} \quad N^2(z) = g \left(\alpha \frac{\partial \Theta}{\partial z} - \beta \frac{\partial S_A}{\partial z} \right) \quad (7)$$

290 Here $N(z)$ is the buoyancy frequency and f_0 is the mean Coriolis parameter. Solving the
 291 equation requires only climatological (S_A, Θ, p) and boundary conditions. Traditionally
 292 Eq. (7) was solved assuming a rigid lid and a flat bottom, such that the vertical velocity
 293 $(\partial\phi/\partial z)$ vanishes at the upper and lower boundary ($z = 0, -H$) (Kundu et al., 1975; Gill,
 294 1982; Philander, 1978; Wunsch & Stammer, 1997; Nurser & Bacon, 2014). However, recent
 295 studies argue that bottom topography suppresses the deep flow (de La Lama et al., 2016;
 296 LaCasce, 2017), so that it is preferable to solve Eq. (7) with no horizontal flow at the
 297 bottom instead (i.e. $\phi(z = -H) = 0$). With realistic stratification, Eq. (7) is solved
 298 numerically using a fourth-order Runge-Kutta step to integrate downward from the surface
 299 from an initial guess, with adjustments to the eigenvalue made by using Newton's method
 300 until the bottom boundary condition is satisfied. The gravest resulting mode, the "First
 301 Surface Mode", resembles the "equivalent-barotropic" structure (Killworth, 1992) in that
 302 it decays from the surface to the bottom without changing sign. The surface mode also
 303 closely resembles the primary EOF from current meter observations, which often accounts
 304 for 50-90% of the variance (de La Lama et al., 2016; LaCasce & Groeskamp, 2020). The
 305 deformation radius is then given by Eq. (4) (Fig. 5a). We also solve Eq. (7) for the
 306 traditional flat-bottom boundary condition to obtain ϕ_{flat} . We use $|\phi_{\text{flat}}|$, its associated
 307 deformation radius and a new fit of $\gamma^{-1} = 1.38$ days to obtain the flat-bottom estimate of
 308 K shown in Fig. 1.

309 Acknowledgments

310 TJMcD gratefully acknowledges support from the Australian Research Council through
 311 grant FL150100090, and JHL was supported by the Norwegian Research Council through
 312 project 302743 (The Rough Ocean). Altimetric data analysis was performed using the
 313 PANGEO platform, which was supported by NSF Award 1740648. We thank David Mar-
 314 shall and an anonymous reviewer for their insightful comments that improved this pa-
 315 per. WOA18 data <https://www.nodc.noaa.gov/OC5/woa18/>. GSW toolbox [http://www](http://www.teos-10.org/software.htm)
 316 [.teos-10.org/software.htm](http://www.teos-10.org/software.htm). For the CMEMS data go to [https://resources.marine](https://resources.marine.copernicus.eu/)
 317 [.copernicus.eu/](https://resources.marine.copernicus.eu/), select "data" and use product identifier;
 318 *SEALEVEL_GLO_PHY_L4_REP_OBSERVATIONS_008_047*. The mixing output based on
 319 this study, for the WOA grid, and related matlab scripts are available at [https://figshare](https://figshare.com/articles/Groeskamp_et_al_2020_-_mixing_diffusivities/12554555)
 320 [.com/articles/Groeskamp_et_al_2020_-_mixing_diffusivities/12554555](https://figshare.com/articles/Groeskamp_et_al_2020_-_mixing_diffusivities/12554555).

321 References

- 322 Abernathey, R., Marshall, J., Mazloff, M., & Shuckburgh, E. (2010, 2016/01/27). En-
 323 hancement of mesoscale eddy stirring at steering levels in the southern ocean. *Jour-*
 324 *nal of Physical Oceanography*, *40*(1), 170–184. Retrieved from [http://dx.doi.org/](http://dx.doi.org/10.1175/2009JPO4201.1)
 325 [10.1175/2009JPO4201.1](http://dx.doi.org/10.1175/2009JPO4201.1) doi: 10.1175/2009JPO4201.1
- 326 Abernathey, R. P., & Marshall, J. (2013). Global surface eddy diffusivities derived from
 327 satellite altimetry. *Journal of Geophysical Research: Oceans*, *118*(2), 901–916. doi:
 328 [10.1002/jgrc.20066](https://doi.org/10.1002/jgrc.20066)
- 329 Adcroft, A., Anderson, W., Balaji, V., Blanton, C., Bushuk, M., Dufour, C. O., ... Zhang,
 330 R. (2019). The gfdl global ocean and sea ice model om4.0: Model description and
 331 simulation features. *Journal of Advances in Modeling Earth Systems*, *11*(10), 3167–
 332 3211. doi: 10.1029/2019MS001726
- 333 Armi, L., & Stommel, H. (1983). Four views of a portion of the north atlantic sub-
 334 tropical gyre. *Journal of Physical Oceanography*, *13*(5), 828–857. doi: 10.1175/
 335 [1520-0485\(1983\)013\(0828:FVOAPO\)2.0.CO;2](https://doi.org/10.1175/1520-0485(1983)013(0828:FVOAPO)2.0.CO;2)

- 336 Barker, P. M., & McDougall, T. J. (2017). Stabilizing hydrographic profiles with minimal
337 change to the water masses. *Journal of Atmospheric and Oceanic Technology*, *34*(9),
338 1935–1945. doi: 10.1175/JTECH-D-16-0111.1
- 339 Barker, P. M., & McDougall, T. J. (2020). Two interpolation methods using multiply-
340 rotated piecewise cubic hermite interpolating polynomials. *Journal of Atmospheric*
341 *and Oceanic Technology*, *37*(4), 605–619. Retrieved from [https://doi.org/10.1175/](https://doi.org/10.1175/JTECH-D-19-0211.1)
342 [JTECH-D-19-0211.1](https://doi.org/10.1175/JTECH-D-19-0211.1) doi: 10.1175/JTECH-D-19-0211.1
- 343 Bretherton, F. P. (1966). Critical layer instability in baroclinic flows. *Quarterly Journal of*
344 *the Royal Meteorological Society*, *92*(393), 325–334. doi: 10.1002/qj.49709239302
- 345 Busecke, J., & Abernathey, R. P. (2019, 01). Ocean mesoscale mixing linked to climate
346 variability. *Science Advances*, *5*(1), eaav5014. doi: 10.1126/sciadv.aav5014
- 347 Busecke, J., Gordon, A. L., Li, Z., Bingham, F. M., & Font, J. (2014). Subtropical surface
348 layer salinity budget and the role of mesoscale turbulence. *Journal of Geophysical*
349 *Research: Oceans*, *119*(7), 4124–4140. doi: 10.1002/2013JC009715
- 350 Canuto, V. M., Cheng, Y., Howard, A. M., & Dubovikov, M. S. (2019). Three-dimensional,
351 space-dependent mesoscale diffusivity: Derivation and implications. *Journal of Phys-*
352 *ical Oceanography*, *49*(4), 1055–1074. doi: 10.1175/JPO-D-18-0123.1
- 353 Chapman, C., & Sallée, J.-B. (2017). Isopycnal mixing suppression by the antarctic cir-
354 cumpolar current and the southern ocean meridional overturning circulation. *Journal*
355 *of Physical Oceanography*, *47*(8), 2023–2045. doi: 10.1175/JPO-D-16-0263.1
- 356 Charney, J. G. (1971). Geostrophic turbulence. *Journal of the Atmospheric Sciences*, *28*(6),
357 1087–1095. doi: 10.1175/1520-0469(1971)028<1087:GT>2.0.CO;2
- 358 Chelton, D. B., deSzoeke, R. A., Schlax, M. G., El Naggar, K., & Siwertz, N. (1998).
359 Geographical variability of the first baroclinic rossby radius of deformation. *Journal*
360 *of Physical Oceanography*, *28*(3), 433–460. doi: 10.1175/1520-0485(1998)028<0433:
361 GVOTFB>2.0.CO;2
- 362 Chelton, D. B., & Schlax, M. G. (1996). Global observations of oceanic rossby waves.
363 *Science*, *272*(5259), 234–238.
- 364 Cole, S. T., Wortham, C., Kunze, E., & Owens, W. B. (2015). Eddy stirring and horizontal
365 diffusivity from argo float observations: Geographic and depth variability. *Geophysical*
366 *Research Letters*, *42*(10), 3989–3997. doi: 10.1002/2015GL063827
- 367 de La Lama, M. S., LaCasce, J. H., & Fuhr, H. K. (2016, 09). The vertical structure of
368 ocean eddies. *Dynamics and Statistics of the Climate System*, *1*(1). doi: 10.1093/
369 climsys/dzw001
- 370 Dewar, W. K. (1986). Mixed layers in gulf stream rings. *Dynamics of Atmospheres and*
371 *Oceans*, *10*(1), 1–29. doi: [https://doi.org/10.1016/0377-0265\(86\)90007-2](https://doi.org/10.1016/0377-0265(86)90007-2)
- 372 Durrieu De Madron, X., & Weatherly, G. (1994). Circulation, transport and bottom bound-
373 ary layers of the deep currents in the brazil basin. *Journal of Marine Research*, *52*(4),
374 583–638. doi: doi:10.1357/0022240943076975
- 375 Ferrari, R., & Nikurashin, M. (2010, 2019/12/19). Suppression of eddy diffusivity across
376 jets in the southern ocean. *Journal of Physical Oceanography*, *40*(7), 1501–1519. doi:
377 10.1175/2010JPO4278.1
- 378 Ferreira, D., Marshall, J., & Heimbach, P. (2005, 2014/08/19). Estimating Eddy Stresses by
379 Fitting Dynamics to Observations Using a Residual-Mean Ocean Circulation Model
380 and Its Adjoint. *Journal of Physical Oceanography*, *35*(10), 1891–1910. Retrieved
381 from <http://dx.doi.org/10.1175/JP02785.1> doi: 10.1175/JPO2785.1
- 382 Fox-Kemper, B., Adcroft, A., Böning, C. W., Chassignet, E. P., Curchitser, E., Danabasoglu,
383 G., . . . Yeager, S. G. (2019). Challenges and prospects in ocean circulation models.
384 *Frontiers in Marine Science*, *6*, 65. doi: 10.3389/fmars.2019.00065
- 385 Garcia, H., Boyer, T., Baranova, O., Locarnini, R., Mishonov, A., Grodsky, A., . . . M.M., Z.
386 (2019). *World ocean atlas 2018: Product documentation* (Tech. Rep.). A. Mishonov,
387 Technical Editor.
- 388 Garzoli, S. L., Gordon, A. L., Kamenkovich, V., Pillsbury, D., & Duncombe-Rae, C. (1996).
389 Variability and sources of the southeastern atlantic circulation. *Journal of Marine*
390 *Research*, *54*(6), 1039–1071.

- 391 Gill, A. E. (1982). *Atmosphere-ocean dynamics*. Academic Press.
- 392 Gill, A. E., Green, J. S. A., & Simmons, A. J. (1974). Energy partition in the
393 large-scale ocean circulation and the production of mid-ocean eddies. *Deep Sea*
394 *Research and Oceanographic Abstracts*, 21(7), 499–528. Retrieved from [http://](http://www.sciencedirect.com/science/article/pii/0011747174900102)
395 www.sciencedirect.com/science/article/pii/0011747174900102 doi: [http://](http://dx.doi.org/10.1016/0011-7471(74)90010-2)
396 [dx.doi.org/10.1016/0011-7471\(74\)90010-2](http://dx.doi.org/10.1016/0011-7471(74)90010-2)
- 397 Gnanadesikan, A., Pradal, M.-A., & Abernathey, R. (2015). Isopycnal mixing by mesoscale
398 eddies significantly impacts oceanic anthropogenic carbon uptake. *Geophysical Re-*
399 *search Letters*, 42(11), 4249–4255. doi: 10.1002/2015GL064100
- 400 Graham, F. S., & McDougall, T. J. (2013, 2013/09/10). Quantifying the Nonconserva-
401 tive Production of Conservative Temperature, Potential Temperature, and Entropy.
402 *Journal of Physical Oceanography*, 43(5), 838–862. doi: 10.1175/JPO-D-11-0188.1
- 403 Groeskamp, S., Sloyan, B. M., Zika, J. D., & McDougall, T. J. (2017, 2017/03/20). Mixing
404 inferred from an ocean climatology and surface fluxes. *Journal of Physical Oceanog-*
405 *raphy*, 47(3), 667–687. doi: 10.1175/JPO-D-16-0125.1
- 406 Hallberg, R. (2013). Using a resolution function to regulate parameterizations of oceanic
407 mesoscale eddy effects. *Ocean Modelling*, 72, 92–103. doi: [https://doi.org/10.1016/](https://doi.org/10.1016/j.ocemod.2013.08.007)
408 [j.ocemod.2013.08.007](https://doi.org/10.1016/j.ocemod.2013.08.007)
- 409 Hautala, S. L. (2018). The abyssal and deep circulation of the Northeast Pacific Basin.
410 *Progress in Oceanography*, 160, 68–82.
- 411 Holloway, G. (1986, 09 18). Estimation of oceanic eddy transports from satellite altime-
412 try. *Nature*, 323(6085), 243–244. Retrieved from [http://dx.doi.org/10.1038/](http://dx.doi.org/10.1038/323243a0)
413 [323243a0](http://dx.doi.org/10.1038/323243a0)
- 414 IOC, SCOR, & IAPSO. (2010). The international thermodynamic equation of seawater –
415 2010: Calculation and use of thermodynamic properties. [Computer software manual].
416 [Available online at www.TEOS-10.org].
- 417 Jackett, D. R., & McDougall, T. J. (1997). A Neutral Density Variable for the World’s
418 Oceans. *Journal of Physical Oceanography*, 27(2), 237–263. doi: 10.1175/1520-
419 -0485(1997)027<0237:ANDVFT>2.0.CO;2
- 420 Jansen, M. F., Adcroft, A., Khani, S., & Kong, H. (2019). Toward an energetically consis-
421 tent, resolution aware parameterization of ocean mesoscale eddies. *Journal of Advances*
422 *in Modeling Earth Systems*, 11(8), 2844–2860. doi: 10.1029/2019MS001750
- 423 Jenkins, W. J. (1987). 3h and 3he in the beta triangle: Observations of gyre ventilation
424 and oxygen utilization rates. *Journal of Physical Oceanography*, 17(6), 763–783. doi:
425 10.1175/1520-0485(1987)017<0763:AITBTO>2.0.CO;2
- 426 Jenkins, W. J. (1998). Studying subtropical thermocline ventilation and circulation using
427 tritium and 3he. *Journal of Geophysical Research: Oceans*, 103(C8), 15817–15831.
428 doi: 10.1029/98JC00141
- 429 Jones, C. S., & Abernathey, R. P. (2019). Isopycnal mixing controls deep ocean ventilation.
430 *Geophysical Research Letters*, 46(22), 13144–13151. doi: 10.1029/2019GL085208
- 431 Joyce, T. M., Luyten, J. R., Kubryakov, A., Bahr, F. B., & Pallant, J. S. (1998). Meso-
432 to large-scale structure of subducting water in the subtropical gyre of the eastern
433 north atlantic ocean. *Journal of Physical Oceanography*, 28(1), 40–61. doi: 10.1175/
434 1520-0485(1998)028<0040:MTLSSO>2.0.CO;2
- 435 Killworth, P. D. (1992, 11). An Equivalent-Barotropic Mode in the Fine Resolu-
436 tion Antarctic Model. *Journal of Physical Oceanography*, 22(11), 1379–1387. doi:
437 10.1175/1520-0485(1992)022<1379:AEBMIT>2.0.CO;2
- 438 Klocker, A., & Abernathey, R. (2013, 2014/08/19). Global Patterns of Mesoscale Eddy
439 Properties and Diffusivities. *Journal of Physical Oceanography*, 44(3), 1030–1046.
440 doi: 10.1175/JPO-D-13-0159.1
- 441 Klocker, A., Ferrari, R., & LaCasce, J. H. (2012, 2019/12/19). Estimating suppression of
442 eddy mixing by mean flows. *Journal of Physical Oceanography*, 42(9), 1566–1576. doi:
443 10.1175/JPO-D-11-0205.1
- 444 Klocker, A., & Marshall, D. P. (2014, 2019/11/11). Advection of baroclinic eddies by
445 depth mean flow. *Geophysical Research Letters*, 41(10), 3517–3521. doi: 10.1002/

- 2014GL060001
- 446 Kundu, P. K., Allen, J. S., & Smith, R. L. (1975). Modal decomposition of the velocity
447 field near the oregon coast. *Journal of Physical Oceanography*, 5(4), 683–704. doi:
448 10.1175/1520-0485(1975)005<0683:MDOTVF>2.0.CO;2
- 449 LaCasce, J. H. (2017). The prevalence of oceanic surface modes. *Geophysical Research*
450 *Letters*, 44(21), 11,097–11,105. doi: 10.1002/2017GL075430
- 451 LaCasce, J. H., Ferrari, R., Marshall, J., Tulloch, R., Balwada, D., & Speer, K. (2014).
452 Float-derived isopycnal diffusivities in the dimes experiment. *Journal of Physical*
453 *Oceanography*, 44(2), 764–780. Retrieved from [http://dx.doi.org/10.1175/JPO-D-](http://dx.doi.org/10.1175/JPO-D-13-0175.1)
454 [13-0175.1](http://dx.doi.org/10.1175/JPO-D-13-0175.1) doi: 10.1175/JPO-D-13-0175.1
- 455 LaCasce, J. H., & Groeskamp, S. (2020, 08). Baroclinic modes over rough bathymetry
456 and the surface deformation radius. *Journal of Physical Oceanography*, 1-40. doi:
457 10.1175/JPO-D-20-0055.1
- 458 Lagerloef, G. S. E., Mitchum, G. T., Lukas, R. B., & Niiler, P. P. (1999). Tropical pacific
459 near-surface currents estimated from altimeter, wind, and drifter data. *Journal of*
460 *Geophysical Research: Oceans*, 104(C10), 23313–23326. doi: 10.1029/1999JC900197
- 461 Ledwell, J. R., Watson, A. J., & Law, C. S. (1993, 08 19). Evidence for slow mixing across
462 the pycnocline from an open-ocean tracer-release experiment. *Nature*, 364(6439),
463 701–703. Retrieved from <http://dx.doi.org/10.1038/364701a0>
- 464 Ledwell, J. R., Watson, A. J., & Law, C. S. (1998). Mixing of a tracer in the pycnocline.
465 *Journal of Geophysical Research: Oceans*, 103(C10), 21499–21529. Retrieved from
466 <http://dx.doi.org/10.1029/98JC01738> doi: 10.1029/98JC01738
- 467 Marshall, D. P., & Adcroft, A. J. (2010). Parameterization of ocean eddies: Potential
468 vorticity mixing, energetics and arnold's first stability theorem. *Ocean Modelling*,
469 32(3), 188–204. doi: <https://doi.org/10.1016/j.ocemod.2010.02.001>
- 470 McDougall, T., & Barker, P. M. (2011). Getting started with TEOS-10 and the Gibbs
471 Seawater (GSW) Oceanographic Toolbox. [Computer software manual]. WG127, ISBN
472 978-0-646-55621-5.
- 473 McDougall, T. J. (2003, 2011/08/21). Potential Enthalpy: A Conservative Oceanic Variable
474 for Evaluating Heat Content and Heat Fluxes. *Journal of Physical Oceanography*,
475 33(5), 945–963. doi: 10.1175/1520-0485(2003)033<0945:PEACOV>2.0.CO;2
- 476 McDougall, T. J., Jackett, D. R., Millero, F. J., Pawlowicz, R., & Barker, P. M. (2012). A
477 global algorithm for estimating Absolute Salinity. *Ocean Science*, 8(6), 1117–1128.
- 478 McDougall, T. J., & McIntosh, P. C. (2001, 2013/01/31). The Temporal-Residual-Mean
479 Velocity. Part II: Isopycnal Interpretation and the Tracer and Momentum Equations.
480 *Journal of Physical Oceanography*, 31(5), 1222–1246. doi: 10.1175/1520-0485(2001)
481 031<1222:TTRMVP>2.0.CO;2
- 482 Meijers, A. J. S. (2014, 07). The southern ocean in the coupled model intercomparison
483 project phase 5. *Philosophical transactions. Series A, Mathematical, physical, and*
484 *engineering sciences*, 372(2019), 20130296–20130296. doi: 10.1098/rsta.2013.0296
- 485 Naveira Garabato, A. C., Polzin, K. L., Ferrari, R., Zika, J. D., & Forryan, A. (2015). A
486 microscale view of mixing and overturning across the antarctic circumpolar current.
487 *Journal of Physical Oceanography*, 46(1), 233–254. Retrieved from [https://doi.org/](https://doi.org/10.1175/JPO-D-15-0025.1)
488 [10.1175/JPO-D-15-0025.1](https://doi.org/10.1175/JPO-D-15-0025.1) doi: 10.1175/JPO-D-15-0025.1
- 489 Nurser, A., & Bacon, S. (2014, November). The rossby radius in the arctic ocean. *Ocean*
490 *Science*, 10(6), 967–975.
- 491 Pedlosky, J. (1987). *Geophysical fluid dynamics*. Springer Science & Business Media.
- 492 Philander, S. G. H. (1978). Forced oceanic waves. *Reviews of Geophysics*, 16(1), 15–46.
493 doi: 10.1029/RG016i001p00015
- 494 Pradal, M.-A., & Gnanadesikan, A. (2014). How does the redi parameter for mesoscale
495 mixing impact global climate in an earth system model? *Journal of Advances in*
496 *Modeling Earth Systems*, 6(3), 586–601. doi: 10.1002/2013MS000273
- 497 Prandtl, L. (1925). Report on investigation of developed turbulence. *Mechanik*, 5(2).
- 498 Pujol, M. I., Faugère, Y., Taburet, G., Dupuy, S., Pelloquin, C., Ablain, M., & Picot, N.
499 (2016, 09). Duacs dt2014: the new multi-mission altimeter data set reprocessed over
500

- 501 20 years. *Ocean Sci.*, 12(5), 1067–1090. doi: 10.5194/os-12-1067-2016
- 502 Redi, M. H. (1982). Oceanic Isopycnal Mixing by Coordinate Rotation. *Journal of Physical*
 503 *Oceanography*, 12(10), 1154–1158. doi: 10.1175/1520-0485(1982)012<1154:OIMBCR>
 504 2.0.CO;2
- 505 Rhines, P. (1970, 06). Edge-, bottom-, and rossby waves in a rotating stratified fluid.
 506 *Geophysical Fluid Dynamics*, 1(3-4), 273–302. doi: 10.1080/03091927009365776
- 507 Roach, C. J., Balwada, D., & Speer, K. (2018). Global observations of horizontal mixing from
 508 argo float and surface drifter trajectories. *Journal of Geophysical Research: Oceans*,
 509 123(7), 4560–4575. doi: 10.1029/2018JC013750
- 510 Sijp, W. P., Bates, M., & England, M. H. (2006, 2012/08/15). Can Isopycnal Mixing Control
 511 the Stability of the Thermohaline Circulation in Ocean Climate Models? *Journal of*
 512 *Climate*, 19(21), 5637–5651. Retrieved from <http://dx.doi.org/10.1175/JCLI3890>
 513 .1 doi: 10.1175/JCLI3890.1
- 514 Smith, K. S., & Marshall, J. (2009). Evidence for enhanced eddy mixing at middepth in
 515 the southern ocean. *Journal of Physical Oceanography*, 39(1), 50–69. doi: 10.1175/
 516 2008JPO3880.1
- 517 Spall, M. A., Richardson, P. L., & Price, J. (1993). Advection and eddy mix-
 518 ing in the mediterranean salt tongue. *Journal of Marine Research*, 51(4), 797-
 519 818. Retrieved from [https://www.ingentaconnect.com/content/jmr/jmr/1993/
 520 00000051/00000004/art00004](https://www.ingentaconnect.com/content/jmr/jmr/1993/00000051/00000004/art00004) doi: doi:10.1357/0022240933223882
- 521 Taburet, G., Sanchez-Roman, A., Ballarotta, M., Pujol, M. I., Legeais, J. F., Fournier,
 522 F., ... Dibarboure, G. (2019, 09). Duacs dt2018: 25 years of reprocessed sea level
 523 altimetry products. *Ocean Sci.*, 15(5), 1207–1224. doi: 10.5194/os-15-1207-2019
- 524 Thompson, R. O., & Luyten, J. R. (1976). Evidence for bottom-trapped topographic rossby
 525 waves from single moorings. *Deep Sea Research and Oceanographic Abstracts*, 23(7),
 526 629 - 635. doi: [https://doi.org/10.1016/0011-7471\(76\)90005-X](https://doi.org/10.1016/0011-7471(76)90005-X)
- 527 Tulloch, R., Ferrari, R., Jahn, O., Klocker, A., LaCasce, J., Ledwell, J. R., ... Watson, A.
 528 (2014). Direct estimate of lateral eddy diffusivity upstream of drake passage. *Journal*
 529 *of Physical Oceanography*, 44(10), 2593–2616.
- 530 Wang, L., Jansen, M., & Abernathy, R. (2016, 2019/12/19). Eddy phase speeds in a
 531 two-layer model of quasigeostrophic baroclinic turbulence with applications to ocean
 532 observations. *Journal of Physical Oceanography*, 46(6), 1963–1985. Retrieved from
 533 <https://doi.org/10.1175/JPO-D-15-0192.1> doi: 10.1175/JPO-D-15-0192.1
- 534 Wunsch, C. (2015). *Modern observational physical oceanography: understanding the global*
 535 *ocean*. Princeton University Press.
- 536 Wunsch, C., & Ferrari, R. (2004). Vertical mixing, energy, and the general circulation
 537 of the oceans. *Annual Review of Fluid Mechanics*, 36(1), 281-314. doi: 10.1146/
 538 annurev.fluid.36.050802.122121
- 539 Wunsch, C., & Stammer, D. (1997). Atmospheric loading and the oceanic “inverted barom-
 540 eter” effect. *Reviews of Geophysics*, 35(1), 79–107. doi: 10.1029/96RG03037
- 541 Zhurbas, V., & Oh, I. S. (2004). Drifter-derived maps of lateral diffusivity in the Pacific
 542 and Atlantic Oceans in relation to surface circulation patterns. *Journal of Geophysical*
 543 *Research: Oceans*, 109(C5), C05015. Retrieved from [http://dx.doi.org/10.1029/
 544 2003JC002241](http://dx.doi.org/10.1029/2003JC002241) doi: 10.1029/2003JC002241
- 545 Zika, J. D., & McDougall, T. J. (2008, 2012/04/10). Vertical and lateral mixing pro-
 546 cesses deduced from the mediterranean water signature in the north atlantic. *Jour-
 547 nal of Physical Oceanography*, 38(1), 164–176. Retrieved from [http://dx.doi.org/
 548 10.1175/2007JP03507.1](http://dx.doi.org/10.1175/2007JP03507.1) doi: 10.1175/2007JPO3507.1
- 549 Zika, J. D., McDougall, T. J., & Sloyan, B. M. (2010, 2011/09/28). Weak Mixing in
 550 the Eastern North Atlantic: An Application of the Tracer-Contour Inverse Method.
 551 *Journal of Physical Oceanography*, 40(8), 1881–1893. doi: 10.1175/2010JPO4360.1
- 552 Zika, J. D., Sallée, J. B., Meijers, A. J. S., Naveira-Garabato, A. C., Watson, A. J., Messias,
 553 M. J., & King, B. A. (2020, 03). Tracking the spread of a passive tracer through
 554 southern ocean water masses. *Ocean Sci.*, 16(2), 323–336. doi: 10.5194/os-16-323-
 555 -2020